Quantum Sensors for Fundamental Physics I
Electromagnetic Resonant Detection

Yifan Chen
yifan.chen@nbi.ku.dk

ITP-CAS, NBI

20 July 2022, online

2022 Summer School of Dark Matter and New Physics

Outlines

Motivation and Introduction to Ultralight Bosons and High-Frequency Gravitational Waves

Ultralight Bosons: $\Psi = a, B^\mu$ and $H^{\mu\nu}$

$$-\frac{1}{2}\nabla^\mu a \nabla_\mu a - \frac{1}{4}B^{\mu\nu}B_{\mu\nu} + \mathcal{L}_{\rm EH}(H) - V(\Psi)$$

- **Extra dimensions** predict a wide range of ultralight boson mass.
  Dimensional reduction from higher form fields:
  e.g. $g^{MN}(5D) \to g^{\mu\nu}(4D) + B^\mu(4D), \quad B^M(5D) \to B^\mu(4D) + a(4D)$.

- String axiverse/photiverse: logarithmic mass window.
  In $4D$, $m_\Psi \propto e^{-\mathcal{V}_{6D}}$.

- Ultralight m_Ψ as low as $\sim 10^{-22}$ eV can be naturally predicted.
  Solution to small-scale problems in the galaxy?

- **Coherent waves** dark matter candidates when $m_\Psi < 1$ eV:

$$\Psi(x^\mu) \simeq \Psi_0(\mathbf{x}) \cos \omega t; \qquad \Psi_0 \simeq \frac{\sqrt{\rho}}{m_\Psi}; \qquad \omega \simeq m_\Psi.$$

Oscillating Ultralight Boson Background

$$\Psi(x^\mu) \simeq \Psi_0(\mathbf{x}) \cos \omega t; \qquad \Psi_0 \simeq \frac{\sqrt{\rho}}{m_\Psi}; \qquad \omega \simeq m_\Psi .$$

- **Oscillating field value: observables in standard model (SM) sectors oscillate as well**:

  Dilaton: coupling constant, mass...

  Axion: EDM, chiral dispersion of photon...

- **The interactions with SM are suppressed by high scale.**

- **Amplifications of the signals:**

  Tabletop experiments on earth: $\rho_{\rm DM} \sim 0.4\ \mathrm{GeV/cm^3}$;

  Astrophysical observation: larger ρ, e.g., galaxy center or near Kerr black hole.

Property of Ultralight Dark Matter

Galaxy formation: virialization $\to \sim 10^{-3}c$ velocity fluctuation, thus kinetic energy $\sim 10^{-6} m_\Psi c^2$.

Effectively coherent waves:

$$\Psi(\vec{x}, t) = \frac{\sqrt{2\rho_\Psi}}{m_\Psi} \cos\left(\omega_\Psi t - \vec{k}_\Psi \cdot \vec{x} + \delta_0\right).$$

- Bandwidth: $\delta\omega_\Psi \simeq m_\Psi \left\langle v^2_{\rm DM} \right\rangle \simeq 10^{-6} m_\Psi$, $Q_\Psi \simeq 10^6$.
- Correlation time: $\tau_\Psi \simeq \mathrm{ms}\, \frac{10^{-6}\mathrm{eV}}{m_\Psi}$.
  Power law detection is used to make integration time longer than τ_Ψ.
- Correlation length: $\lambda_d \simeq 200\ \mathrm{m} \frac{10^{-6}\mathrm{eV}}{m_\Psi} \gg \lambda_c = 1/m_\Psi$.
  Sensor array can be used within λ_d.

Axion/Axion-like Particle

- Axion: hypothetical pseudoscalar motivated by strong CP problem:

Neutron electric dipole $|\bar{\theta}|10^{-16}$ **e.cm is smaller than** 10^{-26} **e.cm.**

$$\bar{\theta} = \theta_{\rm QCD} + \arg\,\det M_u M_d, \qquad \text{Fine tuning!}$$

Why is $\bar{\theta}$ so small? Why 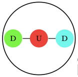

instead of 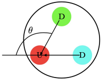

?

Solution: introducing an **dynamical** field with effective potential

$$V \sim -m_a^2 f_a^2 \cos(\bar{\theta} + \frac{a}{f_a}).$$

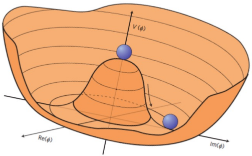

Misalignment Production of Axion

$$\ddot{a} + 3H\dot{a} + m_a^2(T)a = 0.$$

- After $\cancel{PQ}$, massless axion has an initial field value within the Hubble patch, called **initial misalignment angle** $\theta_i \equiv a_i/f_a$.
- **Cosine potential** was generated when $T < \Lambda_{\mathrm{QCD}}$.

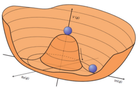 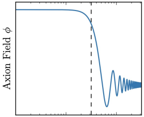

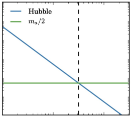

in terms of scale factor.

- $H \gg m_a$, overdamped, $\langle a \rangle = \text{const}$.
- $H \ll m_a$, oscillating with amplitude $\langle a_0 \rangle$ slowly redshifted.
- Non thermal production: **non-relativistic all the time**.

Misalignment Production of QCD Axion

- For QCD axion, $m_a f_a \sim \Lambda_{\rm QCD}^2$ predicts a **thin line in the parameter space**.
- Cosmological parameter: initial misalignment angle $\theta_i \equiv a_i/f_a$.

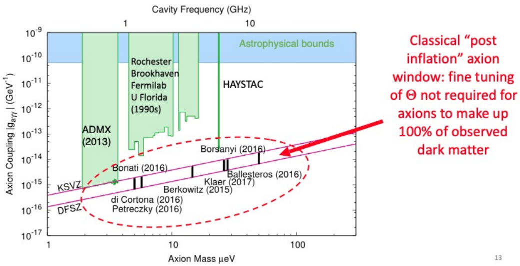

- Assuming $\theta_i \sim 1$ leads to the most natural region of QCD axion dark matter $m_a \sim 10^{-6}\mathrm{eV} \sim$ GHz.
- Different cosmological evolutions can still provide a viable dark matter candidate in other region, e.g., PQ symmetry broken before inflation.

Axion Coupling to the Standard Model

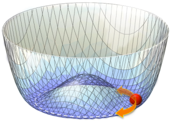

- **Axion Fermion coupling**: $\partial_\mu a \bar{\psi} \gamma^\mu \gamma_5 \psi / f_a$,
  non-linearization of a chiral global symmetry $\sim \partial_\mu a J_5^\mu / f_a$.
  Stellar cooling, DM wind/gradient.

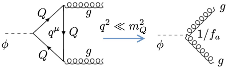

- **Axion Gluon coupling**: $\mathcal{C}_g a \mathrm{Tr} G_{\mu\nu} \tilde{G}^{\mu\nu} / f_a$,
  generated from anomaly/triangle loop diagram.
  Oscillating EDM.

- **Axion Photon coupling**: $\mathcal{C}_\gamma a F_{\mu\nu} \tilde{F}^{\mu\nu} / f_a$,
  from mixing with neutral π_0.
  Photon conversion to axion, inverse Primakoff, birefringence.

Axion QED: Inverse Primakoff Effect

- Axion-photon coupling modifies Maxwell equations:

$$\nabla \cdot \mathbf{E} = \rho - g_{a\gamma} \mathbf{B} \cdot \nabla a$$
$$\nabla \times \mathbf{B} = \partial_t \mathbf{E} + \mathbf{J} - g_{a\gamma} \left(\mathbf{E} \times \nabla a - \mathbf{B} \partial_t a \right)$$

- Background $\vec{B}_0$ and **axion** induces **effective currents**:

$$\vec{J}_{\rm eff} \simeq g_{a\gamma} \vec{B}_0 \sqrt{\rho_{\rm DM}} \cos m_a t.$$

- Inverse Primakoff effect: conversion of axion to an **oscillating EM field** under background $\mathbf{B}_0$.

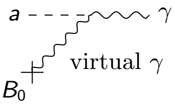

Kinetic Mixing Dark Photon Dark Matter

- A new $U(1)$ vector has kinetic mixing coupling with SM photon:

$$\epsilon F_{\mu\nu} F'^{\mu\nu}.$$

- Similar to axion: extra dimensions, misalignment production, coherent waves.

- Novel aspects: three polarization degrees of freedom, production from inflation.

- In the interaction basis:

$$-\frac{1}{4}\left(\tilde{F}_{\mu\nu}\tilde{F}^{\mu\nu} + \tilde{F}'_{\mu\nu}\tilde{F}'^{\mu\nu}\right) + \frac{1}{2} m_{A'}^2 \tilde{A}'_{\mu}\tilde{A}'^{\mu} - eJ^{\mu}_{\mathrm{EM}}\tilde{A}_{\mu} + \epsilon m_{A'}^2 \tilde{A}_{\mu}\tilde{A}'^{\mu}.$$

  Background dark photon behaves as an **effective current**:

$$J^{\mu}_{\text{eff}} = \epsilon m_{A'}^2 \tilde{A}'^{\mu}.$$

High-Frequency Gravitational Waves

- Gravitational waves above 10 kHz has no know astrophysical origins.

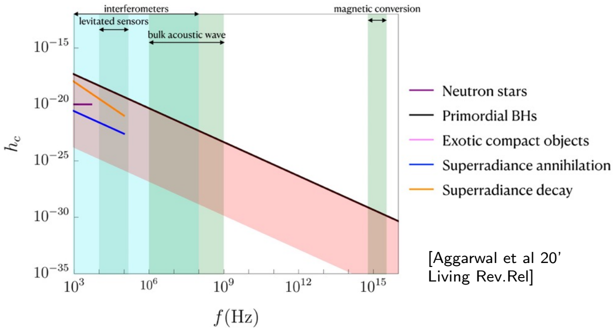

[Aggarwal et al 20' Living Rev.Rel]

- Stochastic background is constrained by N_{eff} during big bang nucleosynthesis (BBN), while a strain is not.
- Inverse Gertsenshtein effect: conversion of $h_{\mu\nu}$ and background EM field to a new **EM field**.

$$\frac{1}{2}h^{\mu\nu}T^{\mathrm{EM}}_{\mu\nu} \to J^{\mu}_{\mathrm{eff}} = \partial_\nu \left(\frac{1}{2} h F^{\mu\nu} + h^{\nu}{}_{\rho} F^{\rho\mu} - h^{\mu}{}_{\rho} F^{\rho\nu} \right) .$$

Electromagnetic Resonant and Broadband Detection

Inverse Primakoff and Haloscope [P.Sikivie 83']

$$\nabla \times \mathbf{B} = \partial_t \mathbf{E} + \mathbf{J} - g_{a\gamma} \left(\mathbf{E} \times \nabla a - \mathbf{B} \partial_t a \right).$$

- Inverse Primakoff: $\mathbf{J}_{\mathrm{eff}}(t) = g_{a\gamma} \mathbf{B}_0 \partial_t a$.
- Sikivie cavity Haloscope:

$$\left(\partial_t^2 + \gamma \partial_t + \omega_{\mathrm{rf}}^2\right) \mathbf{E}_{\mathrm{rf}} = \partial_t \mathbf{J}_{\mathrm{eff}}(t).$$

- Static $\mathbf{B_0}$ and resonant when $\omega_{\mathrm{rf}} = m_a \sim V^{-1/3} \sim \mathcal{O}(1)$ GHz.

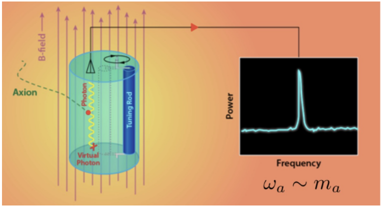

e.g. ADMX, HAYSTACK

Resonant SRF Cavity with AC B Field [A.Berlin, et al 19']

$$\sum_n \left(\partial_t^2 + \gamma\partial_t + \omega_n^2\right) \mathbf{E}_{\rm rf}^n = g_{a\gamma}\partial_t\left(\mathbf{B}\partial_t a\right).$$

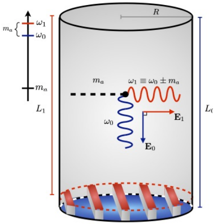

- Using an AC pump mode of $\mathbf{B}_0$:

$$\partial_t(\mathbf{B}_0) \simeq i\omega_0\mathbf{B}_0, \quad \omega_{\rm rf} \simeq \omega_0 + m_a;$$

- Heterodyne upconversion: down to Hz.

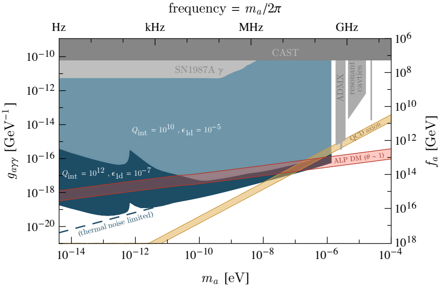

- High $Q_{\rm int} > 10^{10}$ due to the superconducting nature.

Broadband SRF Detection

- Broadband SRF cavity: **two transverse and degenerate modes** with $\omega_{\rm rf} = \omega_0$, down to 10^{-22} eV. [A.Berlin, et al 20']

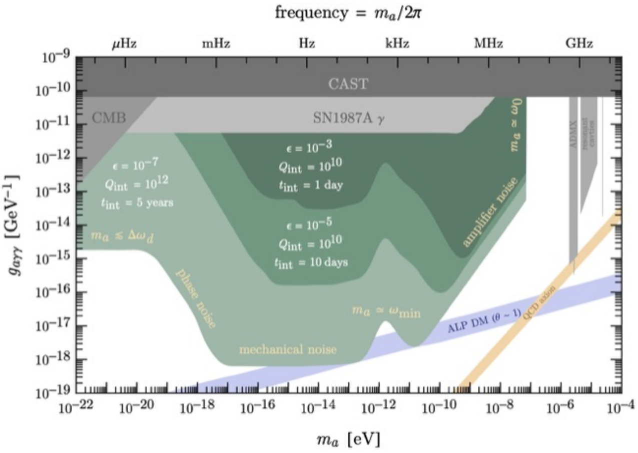

- Highly off-resonant for $m_a >$ kHz.

Effective current induced magnetic field

- In a EM shield room, $\vec{J}_{\mathrm{eff}}$ induce transverse magnetic fields:

$$B \approx |\vec{J}^{\mathrm{eff}}| \; V^{1/3},$$

- For axion and dark photon:

$$\begin{aligned} B_a &\approx 10^{-17}\mathrm{T} \left(\frac{g_{a\gamma}}{10^{-11}\ \mathrm{GeV}^{-1}}\right)\left(\frac{B_0}{1\ \mathrm{T}}\right)\left(\frac{V^{1/3}}{1\ \mathrm{m}}\right), \\ B_{A'} &\approx 10^{-16}\mathrm{T} \left(\frac{\epsilon}{10^{-6}}\right)\left(\frac{m_{A'}}{10\mathrm{Hz}}\right)\left(\frac{V^{1/3}}{1\ \mathrm{m}}\right). \end{aligned}$$

- Strongest magnetic field signal $\propto V^{1/3}$ is at the corner of the room.

Resonant LC circuit

- Resonant conversion happens when $m_\Psi = \omega = \frac{1}{\sqrt{LC}}$.
- Scanning the mass from 100 Hz to 100 MHz by **tuning the capacitor C**.

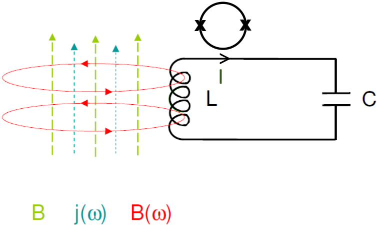

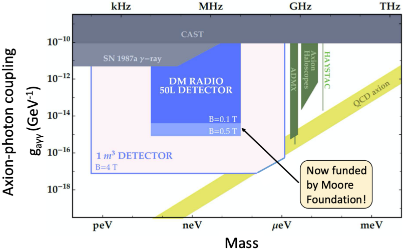

Assumptions: T=10 mK, Q=10^6, 3.5 year integration time, quantum-limited readout

e.g. DM radio, ADMX-SLIC

Broadband LR circuit

- LR circuit: no capacitor, simultaneous scan of broad windows using SQUID. [Y.Kahn, B. Safdi, J. Thaler 16']

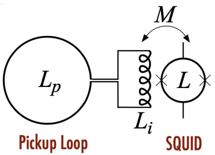

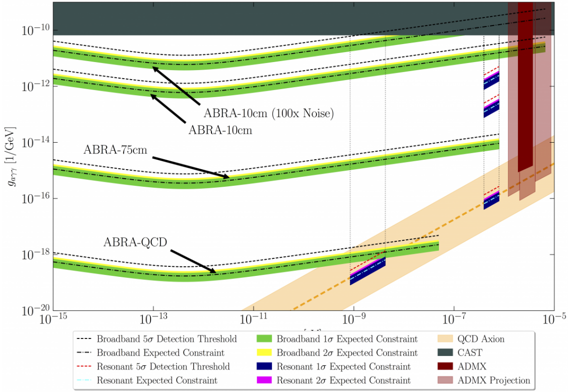

e.g., ABRACADABRA.

Axion QED: Achromatic Birefringence [Carroll, Field, Jackiw 90']

$$\mathcal{L} = -\frac{1}{4}F_{\mu\nu}F^{\mu\nu} - \frac{1}{2}g_{a\gamma}aF_{\mu\nu}\tilde{F}^{\mu\nu} + \frac{1}{2}\partial^\mu a\partial_\mu a - V(a),$$

- Chiral dispersions under axion background:

$$[\partial_t^2 - \nabla^2]A_{L,R} = \mp\, 2g_{a\gamma}n^\mu\partial_\mu a\, k\, A_{L,R}, \qquad \omega_{L,R} \sim k \mp g_{a\gamma}n^\mu\partial_\mu a.$$

n^μ: unit directional vector

- Shift of **electric vector position angle** of linear polarization:

$$\begin{aligned} \Delta\chi &= g_{a\gamma}\int_{\rm emit}^{\rm obs} n^\mu\partial_\mu a\, dl \\ &= g_{a\gamma}[a(t_{\rm obs},\mathbf{x}_{\rm obs}) - a(t_{\rm emit},\mathbf{x}_{\rm emit})], \end{aligned}$$

- Topological effect for each photon: only $a(x^\mu_{\rm emit})$ and $a(x^\mu_{\rm obs})$ dependent.

GW Interferometers and Birefringent Cavity

- Interferometer: rotate EVPA of polarized lasers. [DeRocco, Hook 18']

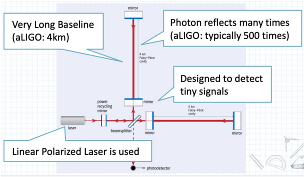

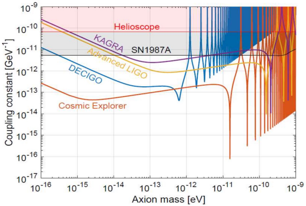

- Birefringent cavity: accumulate the axion-induced sideband. [Liu, Elwood et al 18']

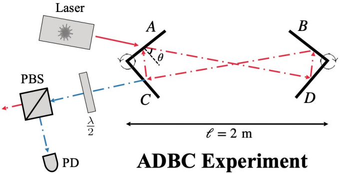

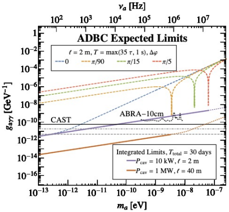

Higher-Frequency Electromagnetic Resonant Detection

Difficult to detect $m_a \gg$ GHz axion dark matter due to short λ_c.

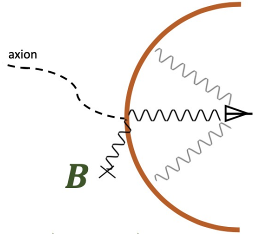

I

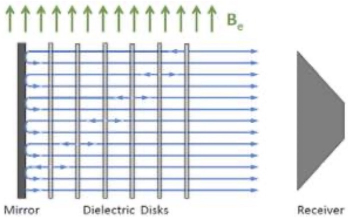

II

Collect all the induced EM emissions:

- I **Dish Antenna**, [Horns et al 12', An et al 22']
- II **Dielectric Haloscope**, e.g., MADMAX. [A.Caldwell et al 17']

Higher-Frequency Electromagnetic Resonant Detection

Difficult to detect $m_a \gg$ GHz axion dark matter due to short λ_c.

III 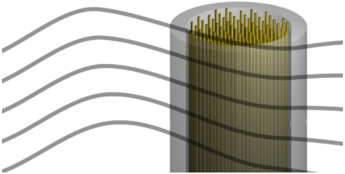

IV 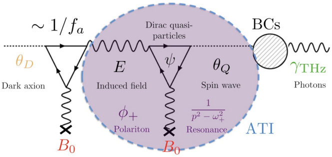

Create resonant states:

- III **Plasma Haloscope**: tunable cryogenic plasma mass, up to 100 GHz. [M.Lawson et al 19']
- IV **Topological Insulator**: quasiparticle polariton, up to THz. [D.J.E.Marsh et al 19']

Standard Quantum Limit for

Single-mode Resonant Systems

Quantization of Cavity Modes

- Quantized EM modes with wavefunctions $\vec{\epsilon}_n(\vec{r})$ In Coulomb gauge:

$$\vec{A} = \sum_n \frac{1}{\sqrt{2\omega_{\rm rf}^n}} \hat{a}_n^\dagger \vec{\epsilon}_n(\vec{r}) e^{-\mathrm{i}\omega_{\rm rf}^n t} + h.c..$$

- The Hamiltonian for each mode reduces to **harmonic oscillator**:

$$H_0 = \frac{1}{2}\int_{\rm V} \left(\vec{E}^2 + \vec{B}^2\right) \mathrm{d}V = \sum_n \omega_{\rm rf}^n \left(\hat{a}_n^\dagger \hat{a}_n + \frac{1}{2}\right),$$

- Interaction with effective currents:

$$H_{\rm int} = \int_{\rm V} \vec{A}\cdot\vec{J}_{\rm eff}\,\mathrm{d}V = \alpha\Psi\left(\hat{a}\, e^{\mathrm{i}\omega_{\rm rf} t} + \hat{a}^\dagger\, e^{-\mathrm{i}\omega_{\rm rf} t}\right)/\sqrt{2},$$

where α contains geometric overlapping factor $\eta_n \propto \int_V \vec{\epsilon}_n \cdot \vec{J}_{\rm eff}\,\mathrm{d}V$.

Quantization of Circuit Modes

- Energy stored in an inductor and a capacitor:

$$H_0 = \frac{\Phi^2}{2L} + \frac{Q^2}{2C} = \omega_{\rm rf}\left(\hat{a}^\dagger \hat{a} + \frac{1}{2}\right).$$

- Interaction with external Φ_Ψ:

$$H_{\rm int} = \frac{\Phi\,\Phi_\Psi}{L} = \alpha\Psi\left(\hat{a}\,e^{{\rm i}\omega_{\rm rf}t} + \hat{a}^\dagger\,e^{-{\rm i}\omega_{\rm rf}t}\right)/\sqrt{2}.$$

- **Circuit representation** of cavity modes with an antenna:

$$\Phi = \int_{\rm Ant} \vec{A}(\vec{r}, t)\cdot {\rm d}\vec{l}.$$

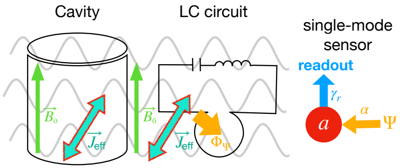

Open quantum system

A system interacting with environment:

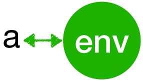

- System mode $\hat{a}$ couples to infinite degrees of freedom $\hat{w}_\omega$:

$$i\hbar\sqrt{2\gamma_r}\int_{-\infty}^{+\infty}\frac{d\omega}{2\pi}[\hat{a}^\dagger\hat{w}_\omega - \hat{a}\hat{w}_\omega^\dagger] + \int_{-\infty}^{+\infty}\frac{d\omega}{2\pi}\hbar\omega\hat{w}_\omega^\dagger\hat{w}_\omega .$$

- Fourier transformation: **0-dim localized mode** $\hat{a}$ couples to an 1-dim bulk w_ξ (transmission line):

$$i\hbar\sqrt{2\gamma_r}\hat{a}^\dagger\hat{w}_{\xi=0} + \mathrm{h.c.} + i\hbar\int_{-\infty}^{+\infty} d\xi\,\hat{w}_\xi^\dagger\partial_\xi\hat{w}_\xi .$$

- Equations of motion for $\hat{a}$ and outgoing mode $\hat{w}_{0_+}$:

$$\dot{\hat{a}} = -\gamma_r\hat{a} + \sqrt{2\gamma_r}\hat{w}_{0_-}; \qquad \hat{w}_{0_+} = \hat{w}_{0_-} - \sqrt{2\gamma_r}\hat{a}$$

Single-mode Resonator as Quantum Sensor

- For a resonator $\hat{a}$ **probing weak signal** Ψ: $\alpha\left(\hat{a}+\hat{a}^{\dagger}\right)\Psi$

- Readout for outgoing mode $\hat{v}_r \equiv \hat{w}_{0_+}$:

$$\hat{v}_r = \frac{\Omega - i\gamma_r}{\Omega + i\gamma_r}\hat{u}_r + \frac{\sqrt{2\gamma_r}\alpha}{\Omega + i\gamma_r}\Psi.$$

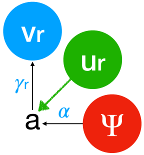

- Fluctuations in incoming mode $\hat{u}_r \equiv \hat{w}_{0_-}$ with quantum limited power spectral density $S_{\rm r} = 1$.

- Resonant signal spectrum $S_{\rm sig} = \frac{\gamma_r\alpha^2}{\gamma_r^2+\Omega^2}\ S_{\Psi}(\Omega)$.

- Trade-off between peak sensitivity and bandwidth by tuning γ_r.

Intrinsic loss and fluctuation

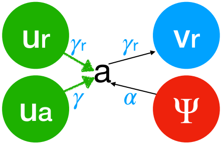

- **Intrinsic loss** $\propto \gamma$ exists, characterized by quality factor $Q_{\rm int} \equiv \omega/\gamma$.

- **Fluctuation-dissipation theorem** predicts intrinsic loss fluctuations

$$S_{\rm int}(\Omega) = \frac{4\gamma\gamma_r}{(\gamma+\gamma_r)^2+\Omega^2}\, n_{\rm occ}.$$

- Using scattering matrix elements:

$$S_{\rm sig} = |S_{0r}|^2 \frac{\alpha^2}{4\gamma} S_\Psi, \qquad S_{\rm noise} = |S_{0r}|^2 n_{\rm occ} + |S_{rr}|^2 \frac{1}{2} + \frac{1}{2}.$$

- **Standard quantum limit for power law detection: resonant $S_{\rm int}$+ flat $S_{\rm r}$**. [Chaudhuri et al 18']

Quantum noise limit for resonant detection

- **Standard quantum limit for power law detection**: [Chaudhuri, Irwin, Graham, Mardon 18']

Noise PSD: resonant intrinsic noise $S_{\rm int}$ + flat readout noise $S_{\rm r}$.

- Sensitivity to $S_{\rm sig}$ and $S_{\rm int}$ is the same.

  SNR^2 $\propto$ range where $S_{\rm int} \gg S_{\rm r}$.

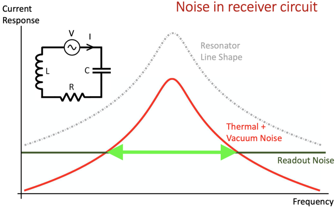

$S_{\rm int} \propto$ Cauchy distribution

- **Beyond quantum limit**:

  Squeezing $S_{\rm r}$, e.g., HAYSTACK.

  Increasing the sensitivity to $S_{\rm sig}$, e.g., white light cavity in optomechanics/GW detection [Miao, Ma, Zhao, Chen 15'].

Standard Quantum Limit for

Multi-mode Resonant Systems

- **Beyond quantum limit of the sensitivity/scan rate?**

Axion Haloscope Array

With $\mathcal{PT}$ Symmetry

based on
arxiv: 2103.12085, Phys. Rev. Res. **4** (2022) no.2, 023015

YC, Minyuan Jiang, Yiqiu Ma, Jing Shu and Yuting Yang

and ongoing

White Light Cavity [X.Li, M.Goryachev, Y.Ma et al 20']

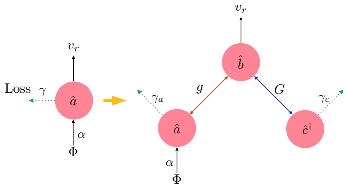

Single Cavity Design

Detector Design with $\mathcal{PT}$ symmetry

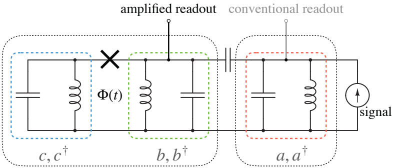

quantum amplifier

conventional detector

Probing mode: $\hbar\alpha(\hat{a}+\hat{a}^\dagger)\Psi$

- **Beam-splitting**: $\hbar g(\hat{a}\hat{b}^\dagger + \hat{a}^\dagger\hat{b})$.
- **Non-degenerate parametric interaction**: $\hbar G(\hat{b}\hat{c} + \hat{b}^\dagger\hat{c}^\dagger)$.
- **$\mathcal{PT}$-symmetry ($\hat{a} \leftrightarrow \hat{c}^\dagger$) emerges** when $g = G$.

$$
\begin{aligned}
(\dot{\hat{a}} + \dot{\hat{c}}^\dagger) &= -i(g-G)\hat{b} - i\alpha\Psi + \cdots; \\
\dot{\hat{b}} &= -\gamma_r\hat{b} - ig(\hat{a}+\hat{c}^\dagger) + \cdots.
\end{aligned}
$$

- Coherent cancellation leads to **double resonance**.
  $S_{\rm sig}$ is largely enhanced when $g \gg$ **intrinsic dissipation** γ:

$$
S_{\rm sig}^{\rm WLC}(\Omega) = \frac{2\gamma_r\alpha^2 S_\Psi(\Omega)}{(\gamma+\gamma_r)^2+\Omega^2}\left(\frac{g^2}{\gamma^2+\Omega^2}\right).
$$

Readout coupling γ_r

Resonator Chain Haloscope

- Generalization to chain detector:

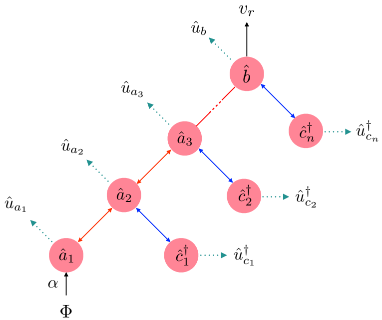

- $\mathcal{PT}$-invariant mode: $\hat{A}_i \equiv \hat{a}_i + \hat{c}_i^\dagger$.

  $\dot{\hat{A}}_1 = -i\alpha\Psi + \cdots\,,$

  $\dot{\hat{A}}_i = -ig\hat{A}_{i-1} + \cdots\,,$

  $\dot{\hat{b}} = -\gamma_r\hat{b} - ig\hat{A}_n.$

  $n+1$-times resonance!

- The whole Hamiltonian is explitly $\mathcal{PT}$ **broken**.

- $S_{\rm sig}$ is n-times enhanced:

$$S_{\rm sig}^{\rm RC}(\Omega) = \frac{2\gamma_r\alpha^2 S_\Psi(\Omega)}{(\gamma+\gamma_r)^2+\Omega^2}\left(\frac{g^2}{\gamma^2+\Omega^2}\right)^n.$$

Binary Tree Haloscope

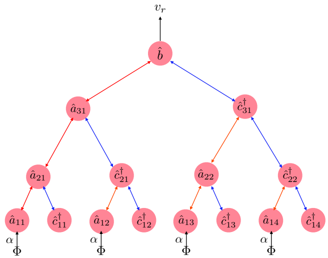

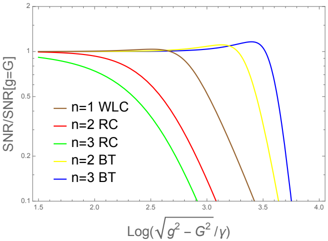

- **Fully $\mathcal{PT}$-symmetric setup** with $\hat{a}_{ij} \leftrightarrow \hat{c}^\dagger_{ij}$ brings strong **robustness**.
- Multi-probing sensors leads to **coherent enhancement**:

$$S^{\mathrm{BT}}_{\mathrm{sig}}(\Omega) = 2^{2n-2} S^{\mathrm{RC}}_{\mathrm{sig}}(\Omega).$$

Quantum Limit for Multi-mode resonators

Scan bandwidth can be significantly increased in a multi-mode system.

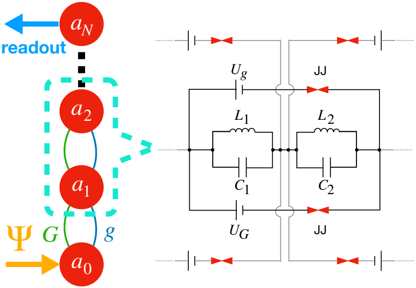

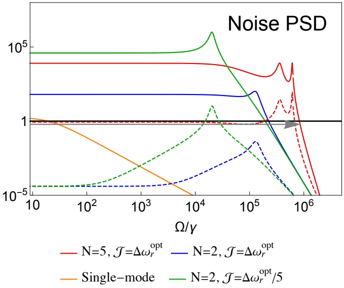

- Far beyond the one of single-mode resonators.
- New quantum limit for multi-mode resonators.

Signal to Noise Ratio and Physics Reach

- $\mathrm{SNR}^2 \propto$ range where $S_{\mathrm{int}} \gg S_{\mathrm{r}} \propto 2^n \left(\frac{g}{\gamma n_{\mathrm{occ}}}\right)^{\frac{2n}{2n+1}}$, where $g/\gamma \to Q_{\mathrm{int}}$.

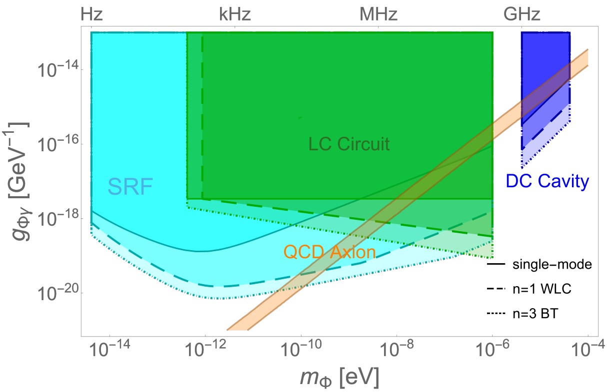

- LC circuit: ineffective at low frequency due to large n_{occ}.

- High Q_{int} and constant n_{occ} for SRF with BT can cover $m_\Psi >$ kHz QCD axion dark matter potentially.

Summary

- Ultralight bosons, especially for QCD axion, are well-motivated.
- Electromagnetic quantum sensor including cavity/circuit can play huge roles in hunting them.
- Quantum limit for resonant detectors: the range where intrinsic fluctuations dominate over readout noise.
- Multi-resonant systems strongly enhances the scan bandwidth and goes beyond the limit of single-mode detectors.

Thank you!

Appendix

Beam splitting coupling

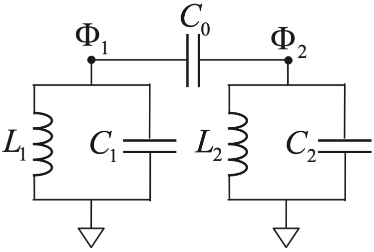

- Use an additional capacitor to couple two LC circuits:

$$H = \frac{1}{2}C_1\dot{\Phi}_1^2 + \frac{1}{2}C_2\dot{\Phi}_2^2 + \frac{1}{2L_1}\Phi_1^2 + \frac{1}{2L_2}\Phi_2^2 + \frac{1}{2}C_0(\dot{\Phi}_1 - \dot{\Phi}_2)^2.$$

- Conjugate momentum to Φ_i involves mixing. Interaction potential:

$$\beta\hbar\sqrt{\omega_1\omega_2}(\hat{a}_1 - \hat{a}_1^\dagger)(\hat{a}_2 - \hat{a}_2^\dagger) \sim \hat{a}_1\hat{a}_2^\dagger + h.c.,$$

Non-Degenerate Parametric amplifier coupling

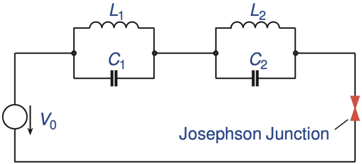

- Use a DC voltage and a Josephson junction to couple two LC circuits:

$$
\begin{aligned}
V &= -\frac{\hbar I_J}{2e_0}\cos\left(\omega_0 t + \frac{2e_0}{\hbar}(\Phi_2 + \Phi_3)\right) \\
&= -\frac{\hbar I_J}{2e_0}\cos\left(\omega_0 t + \kappa_2(a_2 + a_2^\dagger) + \kappa_3(a_3 + a_3^\dagger)\right) \\
&\sim \frac{\hbar I_J}{4e_0}\kappa_2\kappa_3[a_2 a_3 + a_2^\dagger a_3^\dagger],
\end{aligned}
$$